Title

Evolutionary and developmental specialization of foveal cell types in the marmoset

Journal

Proceedings of the National Academy of Sciences of the United States of America, 121(16)

ISSN

0027-8424

Authors

Zhang, Lin
Cavallini, Martina
Wang, Junqiang
et al.

Publication Date

2024-04-16

DOI

10.1073/pnas.2313820121

Peer reviewed

PNAS RESEARCH ARTICLE | NEUROSCIENCE OPEN ACCESS

Evolutionary and developmental specialization of foveal cell types in the marmoset

Lin Zhang[a,1], Martina Cavallini[a,1], Junqiang Wang[a], Ruiqi Xin[a], Qiangge Zhang[b], Guoping Feng[b], Joshua R. Sanes[c], and Yi-Rong Peng[a,2]

Edited by Carol Mason, Columbia University, New York, NY; received August 11, 2023; accepted March 13, 2024

In primates, high-acuity vision is mediated by the fovea, a small specialized central region of the retina. The fovea, unique to the anthropoid lineage among mammals, undergoes notable neuronal morphological changes during postnatal maturation. However, the extent of cellular similarity across anthropoid foveas and the molecular underpinnings of foveal maturation remain unclear. Here, we used high-throughput single-cell RNA sequencing to profile retinal cells of the common marmoset (*Callithrix jacchus*), an early divergent in anthropoid evolution from humans, apes, and macaques. We generated atlases of the marmoset fovea and peripheral retina for both neonates and adults. Our comparative analysis revealed that marmosets share almost all their foveal types with both humans and macaques, highlighting a conserved cellular structure among primate foveas. Furthermore, by tracing the developmental trajectory of cell types in the foveal and peripheral retina, we found distinct maturation paths for each. In-depth analysis of gene expression differences demonstrated that cone photoreceptors and Müller glia (MG), among others, show the greatest molecular divergence between these two regions. Utilizing single-cell ATAC-seq and gene-regulatory network inference, we uncovered distinct transcriptional regulations differentiating foveal cones from their peripheral counterparts. Further analysis of predicted ligand–receptor interactions suggested a potential role for MG in supporting the maturation of foveal cones. Together, these results provide valuable insights into foveal development, structure, and evolution.

marmoset | fovea | scRNA-seq | cone photoreceptor | Müller glia

Significance

The sharpness of our eyesight hinges on a tiny retinal region known as the fovea. The fovea is pivotal for primate vision and is susceptible to diseases like age-related macular degeneration. We studied the fovea in the marmoset—a primate with ancient evolutionary ties. Our data illustrated the cellular and molecular composition of its fovea across different developmental ages. Our findings highlighted a profound cellular consistency among marmosets, humans, and macaques, emphasizing the value of marmosets in vision research and the study of visual diseases.

Diurnal (day-active) anthropoid primates, including monkeys, apes, and humans, are highly visual animals that perceive the world with high spatial and chromatic resolution (1). Nearly all of their high-acuity and most of their chromatic vision is mediated by a small, specialized central region of the retina called the fovea, which is absent from all other mammals and may be the only primate-specific structure in the mammalian brain (2–4) (Fig. 1*A*). Two observations dramatize the importance of the fovea. First, although the fovea occupies only ~1% of the retinal surface, it supplies ~50% of retinal input to the visual cortex (5, 6). Second, injuries or diseases that disable the fovea lead to devastating visual impairment, whereas loss of far larger swaths of peripheral retina has much milder effects (7, 8).

The fundamental cellular plan of the fovea is similar to that of the peripheral retina (9). In both cases, cells comprise six main classes, most of which can be divided into multiple types: photoreceptors (PRs), which sense light; interneurons (horizontal, bipolar, and amacrine cells), which process visual information relayed from PRs; retinal ganglion cells (RGCs), which integrate input from interneurons and send axons through the optic nerve to the rest of the brain; and a single endogenous glial type called the Müller glia (MG) (9, 10). However, the fovea has modified this basic plan with a variety of structural and functional specializations: 1) The fovea, and particularly its central portion, the foveola, are depressed, forming a shallow pit (5, 6) (Fig. 1*B*). 2) The inner nuclear and ganglion cell layers, containing interneurons and RGCs, are displaced, presumably to reduce light scattering. 3) Nearly all PRs in the foveal center are cones, whereas >90% of PRs in the peripheral retina are rods (11, 12). 4) Consistent with cone dominance, bipolar cells that receive input primarily from rods (rod bipolar cells) are sparse in the fovea but the major bipolar type in the periphery (5, 13). 5) The outer segments of foveal cones, which contain the visual pigment (opsin), are far longer and thinner than those in peripheral retina (14). The length enhances sensitivity while the small diameter improves spatial resolution. 6) Likewise, axons of foveal cones are longer than those of peripheral cones, enabling them to reach displaced bipolar and horizontal cell dendrites in the inner nuclear layer (15). 7) Excitatory drive to most foveal RGCs arises from a single PR, whereas peripheral RGCs may receive input from dozens of PRs (5, 6, 11). This arrangement maximizes the spatial resolution of foveal RGCs, albeit at the expense of sensitivity.

Although the anatomical and physiological bases of these specializations have been documented in detail, their molecular correlates remain largely unknown. Here, we have

Author affiliations: [a]Department of Ophthalmology and Stein Eye Institute, David Geffen School of Medicine at University of California Los Angeles, Los Angeles, CA 90095; [b]McGovern Institute for Brain Research, Department of Brain and Cognitive Sciences, Massachusetts Institute of Technology, Cambridge, MA 02139; and [c]Center for Brain Science and Department of Molecular and Cellular Biology, Harvard University, Cambridge, MA 02138

Author contributions: L.Z., J.R.S., and Y.-R.P. designed research; L.Z., M.C., J.W., R.X., Q.Z., and Y.-R.P. performed research; L.Z., J.W., Q.Z., G.F., and Y.-R.P. contributed new reagents/analytic tools; L.Z., M.C., J.W., R.X., and Y.-R.P. analyzed data; Y.-R.P. and J.R.S. provide fundings and resources; and J.R.S. and Y.-R.P. wrote the paper.

The authors declare no competing interest.

This article is a PNAS Direct Submission.

[1]L.Z. and M.C. contributed equally to this work.

[2]To whom correspondence may be addressed. Email: yirongpeng@mednet.ucla.edu.

This article contains supporting information online at https://www.pnas.org/lookup/suppl/doi:10.1073/pnas.2313820121/-/DCSupplemental.

Published April 10, 2024.

used high-throughput single-cell transcriptome profiling (scRNA-seq) to address issues relating to the cell types, development, and evolution of the fovea in the common marmoset (*Callithrix jacchus*). The marmoset is well-suited for this inquiry for three reasons. First, its small size, relatively short gestation time, and genetic accessibility make it useful for developmental studies (16, 17). Second, these features have enabled numerous recent studies of the marmoset visual system, so much is now known about its retina (18–23). Third, New World (*Platyrrhine*) primates including marmosets diverged early in anthropoid evolution (35 to 40 Mya) from Old World (*Catarrhine*) primates, such as macaques, apes, and humans (16, 24, 25) (Fig. 1*A*). Thus, comparison of marmoset fovea with those of macaques and humans can provide insights into how it arose in primates.

Our aim in the work reported here was to learn more about how the fovea arises both in phylogeny, as foveated primates arose from their nonfoveated ancestors, and during ontogeny, as the fovea differentiates from an initially uniform retina. To this end, we generated cell atlases from neonatal and adult marmoset fovea and peripheral retina and compared them to each other and to atlases we had previously generated from adult human and macaque fovea and peripheral retina (26, 27). We found that over 90% of cell types were shared across regions, ages, and species. However, in each case, we found large numbers of genes differentially expressed by shared types. We used a variety of computational methods to gain insight into the biological significance of these differences. Our results highlighted foveal cone photoreceptors and MG as cell types that differ markedly between neonates and adults and between periphery and fovea. Further analysis of these differences suggested that factors derived from MG might promote the maturation of foveal cones.

Results

Cell Atlas of the Adult Marmoset Retina. We generated a cell atlas of the adult (>2-y-old) marmoset fovea and peripheral retina. Cells were dissociated for high -throughput scRNA-seq using the 10X Genomics platform (28) (Fig. 1*C*). Foveal cells were profiled without pretreatment. Peripheral cells were treated with anti-CD73 to deplete rod PRs or with anti-CD90 to enrich RGCs, using methods we had developed in studies of macaque (26). Despite the use of distinct treatments for foveal and peripheral samples, the molecular complexities of cells in both regions are comparable (*SI Appendix*, Fig. S1*A*). We also performed single nucleus RNA-seq (snRNA-seq) on the peripheral retina. After filtering out poor-quality cells or nuclei, we obtained 29,169 foveal and 15,098 peripheral high-quality transcriptomes (*SI Appendix*, Table S1).

Based on unsupervised clustering methods, we divided the foveal cells into six cell classes, which we annotated using known class-specific marker genes (26, 27, 29, 30): PRs, horizontal cells (HCs), bipolar cells (BCs), amacrine cells (ACs), RGCs, and non-neuronal cells (NN) (Fig. 1*D*). From each cell class, we further clustered individual cell types. In total, we identified a total of 68 types: 3 PRs, 2 HCs, 13 BCs, 30 ACs, 16 RGCs, and 4 NN types (Fig. 2*A* and *SI Appendix*, Table S2). Biases associated with specific animal or sample batches were negligible after batch correction (*SI Appendix*, Fig. S1*B*).

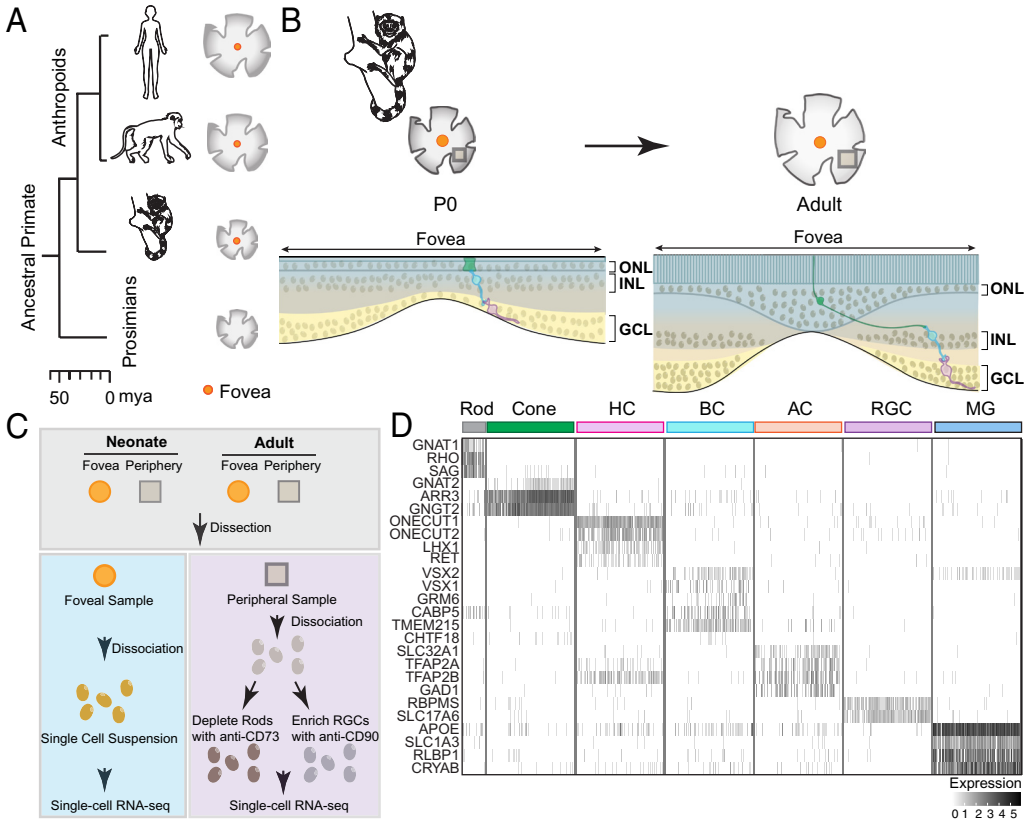

Fig. 1. The evolutionary and developmental formation of the primate fovea. (*A*) Phylogenetic tree of selected primate species illustrating the evolutionary emergence of the fovea in diurnal anthropoids. The scale bar indicates the estimated divergence time in Mya). (*B*) Sketches of the cellular arrangement in the marmoset fovea at the neonatal (*Left*) and adult (*Right*) stages. The midget pathway, consisting of a cone (green), a midget bipolar cell (blue), and a midget ganglion cell (purple) is demonstrated in both neonatal and adult fovea to highlight its developmental change. (*C*) Diagram summarizing the experimental workflow for scRNA-seq analysis. (*D*) Heatmap showing gene expression patterns of marker genes in individual cell classes in the neonatal marmoset fovea.

We verified the clustering result in two ways. First, we asked to what extent the cell types can still be identified without prior separation into cell classes. To this end, we analyzed all foveal cells together and clustered using an iterative unsupervised method with a maximum resolution (*SI Appendix*, *Materials and Methods*). Cell types identified by this method corresponded to those described above (*SI Appendix*, Fig. S1*C*). Second, we analyzed differentially expressed genes (DEGs) and identified markers that are specifically expressed by individual cell types (Fig. 2*C* and *SI Appendix*, Fig. S2). Thus, multiple approaches identified a set of 68 transcriptomically distinguishable foveal cell types.

We clustered peripheral retinal cells obtained by scRNA-seq using similar methods but supplemented them with RGCs and HCs from the snRNA-seq dataset as these two classes had fewer numbers of cells than others (*SI Appendix*, Table S1). We integrated scRNA-seq and snRNA-seq data by canonical correlation analysis (CCA) to overcome potential expression-level shift caused by different preparation methods (31) (*SI Appendix*, Fig. S1 *D* and *E*). We identified a total of 56 types including 3 PRs, 2 HCs, 13 BCs, 16 ACs, 18 RGCs, and 4 NN types (Fig. 2*B*). The smaller number of AC types from periphery compared to fovea likely reflects the poor recovery of glycinergic ACs with CD90 selection (26). Like the foveal dataset, we were able to classify all the cell types using high resolution and identified specific marker genes for individual cell types (*SI Appendix*, Figs. S1*E* and S3). All peripheral types were shared with foveal types in the adult retina (see below).

Evolutionary Modification of Foveal Cell Types across Anthropoids. Marmosets diverged from a common ancestor prior to macaques and humans, which are more closely related to each other than to marmosets (16, 25) (Fig. 1*A*). We compared foveal cell types of the three species as one way of asking whether all foveal cell types were present in the primate ancestor. We performed three comparisons. First, we pooled a maximum of 200 cells per type from each species and used CCA to integrate a total of 23,966 cells, followed by unsupervised clustering. All cells fell into the six canonical cell classes, which can be further classified into known subclasses (e.g., GABAergic and Glycinergic ACs) (32) or types (*SI Appendix*, Fig. S4 *A*–*C*). For RGCs, we distinguished midget, parasol, and intrinsically photosensitive (ip) RGCs (18, 33, 34) but grouped all other minor types as a single subclass. These 26 cell types/subclasses contain cells from all three species without species bias (Fig. 3*A* and *SI Appendix*, Fig. S4 *B* and *C*). We found both conserved and species-specific marker genes in homologous types and subclasses (Fig. 3*A* and *SI Appendix*, Fig. S4*D*).

Second, we compared the transcriptomic distance among homologous cell types across the three primates. Hierarchical clustering of homologous cell types showed that most human and macaque types are more similar to each other than either is to the marmoset type (Fig. 3*A*). We also applied a transcriptomic mapping method to match types based on highly variable genes (HVGs) shared between species. Nearly twice as many marmoset cells favorably matched to macaque as to human types in BC, RGC, and AC classes (*SI Appendix*, Fig. S4*E*).

Third, we analyzed the transcriptomic convergence of homologous foveal cell types based on the correlated expression of HVGs (Fig. 3*B*). All pair-wise comparisons showed >61% correlations, with correlation of homologous types between macaques and humans higher than those in marmoset-human comparisons in 20/25 cases (Fig. 3*B*). Thus, the transcriptomic relationship among foveal cell types mirrors the evolutionary distance among primates (Fig. 1*A*) (25).

We also compared the abundance of foveal cell types among the three species (Fig. 3*A* and *SI Appendix*, Table S3). The abundance of most types was similar across species, but several species-specific enrichments emerged. 1) The abundance of two major cell types in the ON midget pathway–invaginated midget bipolar (IMB) and ON midget ganglion cells (ON_MGC) varies in the order: human > macaque > marmoset, suggesting further enrichment of the foveal ON midget pathway in primates with a higher order. 2) The fraction of cones among all photoreceptors is higher in the human and marmoset fovea than in the macaque fovea. 3) Although the OFFx BC type is absent in marmosets, it has been identified as BC1B in rodents and transcriptomically in several other species, including macaques and humans (26, 35–37). This pattern suggests that the BC1B/OFFx type has been lost in marmosets. Altogether, these results demonstrated that primate foveas share a diverse pool of conserved cell types, but that evolutionary modifications are present in the cellular and molecular composition of foveal cell types.

Cell Atlas of the Neonatal Marmoset Retina. Next, we generated cell atlases from neonatal marmoset fovea and peripheral retina; similar to the adult retina, we profiled all cells from fovea but depleted rods or enriched RGCs from peripheral samples. We did not observe expression-level differences caused by different preparation methods (*SI Appendix*, Fig. S5 *A*, *B*, and *D*). From 21,675 high-quality single-cell foveal transcriptomes, we identified 65 cell types: 3 PRs, 2 HCs, 13 BCs, 28 ACs, 15 RGCs, and 4 NN types; from 22,846 high-quality peripheral transcriptomes, we identified 68 types: 3 PRs, 2 HCs, 13 BCs, 31 ACs, 16 RGCs, and 3 NN types (Fig. 4 *A* and *B* and *SI Appendix*, Table S1). Similar to the adult cell atlas, all cell types identified within individual classes could also be identified through a global clustering of all the cells (*SI Appendix*, Fig. S5 *C* and *E*), and we were able to identify specific marker genes for each cell type (Fig. 4*C* and *SI Appendix*, Figs. S6 and S7).

Cell Types Are Shared between the Fovea and Peripheral Retina and Fully Specified by Birth. We next compared cell types across regions and ages. We applied a transcriptomic mapping method based on a multiclass classification framework using HVGs shared between pairs of datasets (26, 38) (*SI Appendix*, *Materials and Methods*). For this analysis, we included MG but excluded other NN types. There was a nearly complete correspondence between foveal and peripheral types in both neonates and adults (Fig. 5 *A* and *B* and *SI Appendix*, Table S4). However, the low recovery of AC types with the CD90 enrichment method in the adult peripheral sample led to a one-to-multiple match in several cases (Fig. 5*B* and *SI Appendix*, Fig. S5*D* and Table S4). We next asked whether cell types are specified in neonates. Using the same transcriptomic mapping methods, we found that all 62 foveal cell types in the neonatal retina have corresponding types in the adult fovea. Out of these, 59/62 types had a 1:1 match, while two AC types and one RGC type showed a 1:2 match, suggesting a developmental maturation to further diversify these types (Fig. 5*C* and *SI Appendix*, Table S4). Similarly, all 66 peripheral cell types in the neonatal retina correspond to adult peripheral cell types, despite a multiple-to-one match observed in several cases due to the insufficient sampling of adult peripheral AC types (Fig. 5 *C* and *D* and *SI Appendix*, Table S4). Thus, the fovea and peripheral retina share most if not all cell types, and nearly all cell types are present and molecularly specified by birth.

Distinct Developmental Paths of Cell Types in the Fovea and Peripheral Retina. Knowing that most cell types are present across regions and ages, we next analyzed regional (foveal versus peripheral region) and developmental (neonatal versus adult stage) differences between their transcriptomes. To assess the regional differences, we first integrated the cell types shared between the two regions at each age (Fig. 6 *A* and *C* and *SI Appendix*, Table S5).

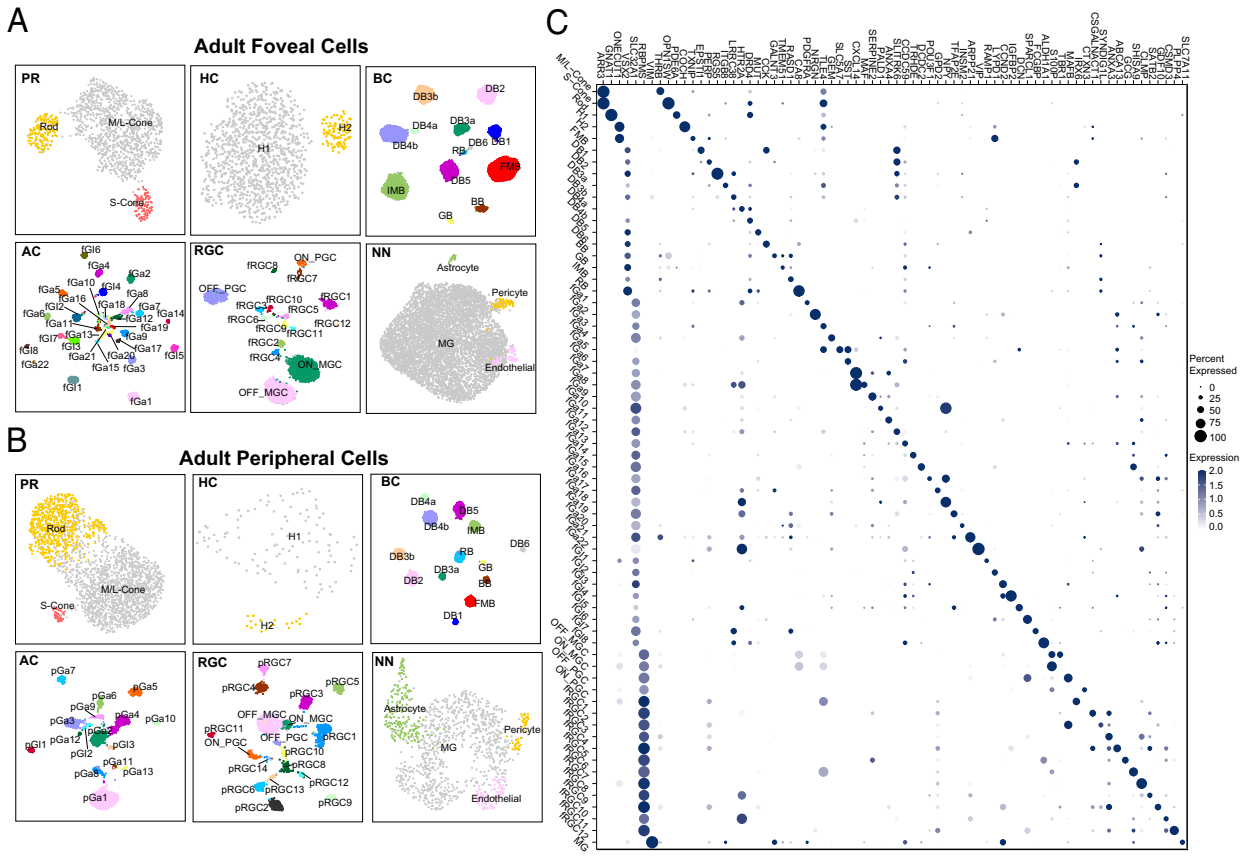

Fig. 2. Cell atlas of the adult marmoset retina. (*A*) Uniform Manifold Approximation and Projection (UMAP) visualization of cell types from individual cell classes (PR, photoreceptors; HC, horizontal cells; BC, bipolar cells; AC, amacrine cells; RGC, retinal ganglion cells; NN, non-neuronal cells) in the fovea of adult marmoset. (*B*) UMAP visualization of cell types from individual cell classes in the peripheral retina of adult marmoset. (*C*) Dot plot showing the expression of marker genes for individual foveal cell classes (*Left* seven columns) and types (remaining columns).

We then used two methods to calculate cell type–specific regional scores. The first was based on a signed gene-set enrichment analysis (sGSEA), which calculates a normalized enrichment score (NES) for genes differentially expressed between corresponding cell types (*SI Appendix*, Fig. S8 *A* and *B* and *Materials and Methods*). A higher NES indicates a greater regional difference. At both ages, only three to four cell types, such as MG and M/L-cones, showed significantly high NES values (Fig. 6 *A* and *C*). Second, we calculated the earth mover's distance (EMD) (39) scores to quantify the similarity between the density distributions of foveal and peripheral cells in terms of the expression of DEGs (*SI Appendix*, Fig. S8 *E* and *F*). A higher EMD score indicates a greater transcriptomic divergence between the corresponding foveal and peripheral types. Consistent with the sGSEA method, only 24% of neonatal cell types and 26% of adult cell types showed a regional difference above the mean change (Fig. 6 *B* and *D*). Therefore, using both methods, we found that the regional difference was not universally present in all cell types, but rather more significant in a small subset of cell types compared to others. Furthermore, we compared the regional differences of all cell types across ages by ranking their statistical significances, transforming the NES into a false discovery rate (FDR)-adjusted *P* value (*SI Appendix*, *Materials and Methods*). We found that in adults, most cell types exhibited more significant regional differences than in the neonates, as determined by –log10FDR values (*SI Appendix*, Fig. S8*C*). Thus, transcriptomic differences between corresponding foveal and peripheral cell types increase during development.

We then assessed the developmental differences between the fovea and peripheral retina. We separately integrated foveal and peripheral cell types across ages and again used sGSEA and EMD as measures (*SI Appendix*, Table S6). In the fovea, only a few cell types exhibited high developmental scores. In contrast, a large proportion of peripheral cell types showed high developmental scores (Fig. 6 *E* and *G*). Similarly, using the EMD calculation, over 52% of cell types in the peripheral retina showed differences above the mean change, while only 26% of cell types in the fovea underwent significant developmental changes (Fig. 6 *F* and *H*). Moreover, although most foveal cell types show a lesser significance in developmental change, as judged by the –log10FDR rankings, certain foveal cell types stood out with comparable significance comparable to the top peripheral peers (*SI Appendix*, Fig. S8*D*). These results demonstrate that there is a global maturation of cell types in the peripheral retina, indicating the peripheral retina is generally immature at birth; however, select foveal cell types still undergo substantial maturation processes during postnatal development.

Conserved and Divergent Regional Differences in Cones and MG across Primates. All four analyses—sGSEA and EMD by region and by age, highlighted cones and MG—they showed the highest degree of regional difference at both ages and were among the top changed cell types across ages in the fovea (Fig. 6 and *SI Appendix*, Fig. S8 *C* and *D*). We therefore focused on these two cell types for our next analyses. Our initial investigation assessed the extent to which regional differences in cones and MG are shared with those in humans and macaques. We curated a set of DEGs in these two cell types, comparing the fovea to the peripheral retina across three primates. We detected many DEGs that are shared among the three species, suggesting conserved roles for these genes in the regional specialization (*SI Appendix*, Fig. S9 *A–D*). However,

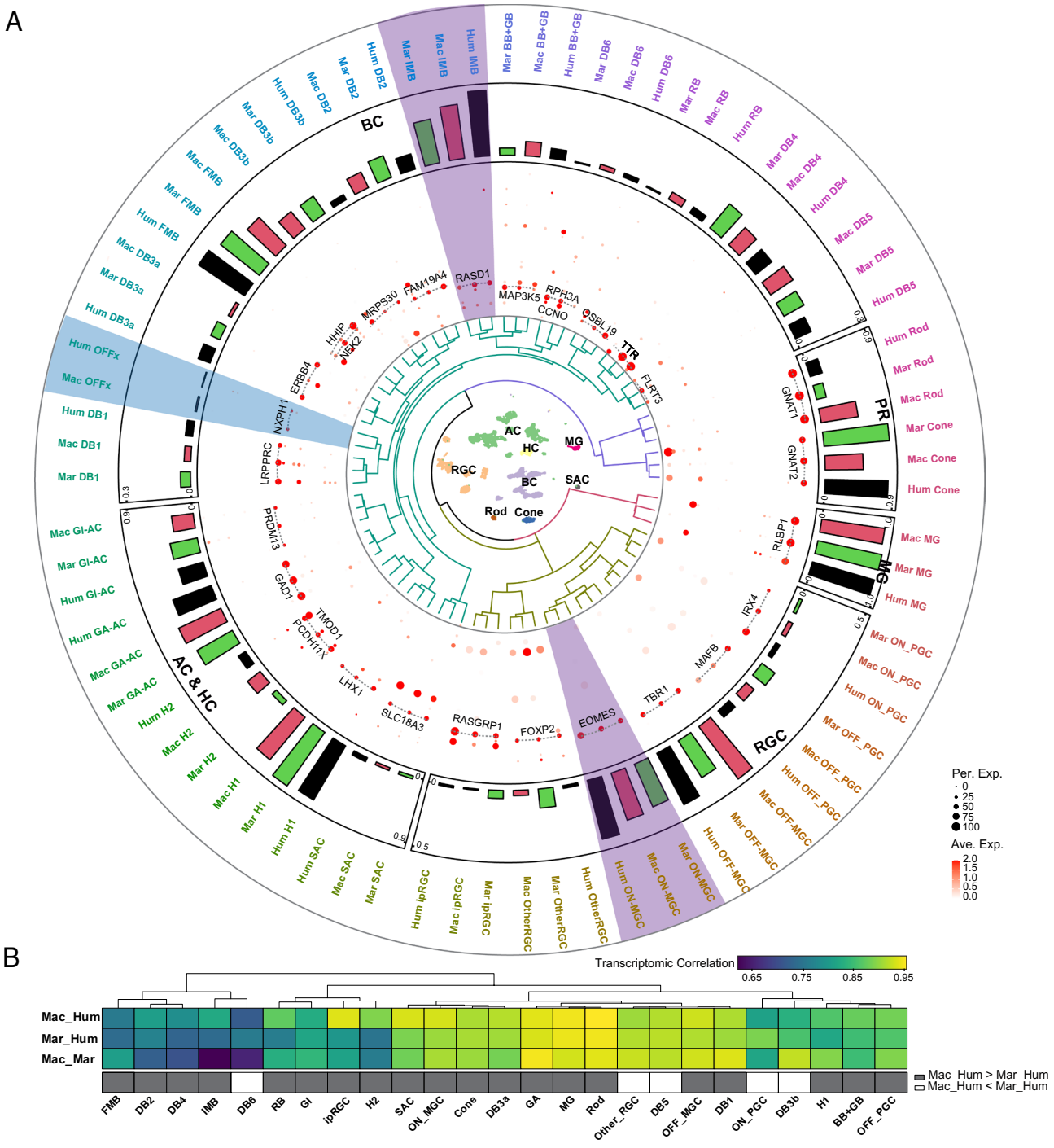

Fig. 3. Conserved and divergent features of foveal cell types across three anthropoid primate species. (*A*) Overview of foveal cell types via comparative analysis of scRNA-seq data from human, macaque, and marmoset. Depicting the plot from inner- to outermost as follows: UMAP of homologous cell types integrated from 23,966 cells across three species; dendrogram of hierarchically related homologous cell types; dot plot showing the expression of conserved marker genes among homologous cell types across species; bar plot showing proportions of cell types within individual cell classes across species, with the maximum proportion within each class indicated at the top edge of the bar plots; 77 homologous cell types. Purple bars highlight ON MGC and IMB, and blue bar highlights the OFFx BC. (*B*) Transcriptomic correlation of homologous cell types between each pair of the three species via Pearson correlation. Gray-filled boxes indicate cell types with a higher correlation between macaque and human, as opposed to marmoset and human, while open boxes indicate the opposite pattern.

each species displayed a larger number of unique DEGs, indicative of molecular divergence and adaptation specific to their foveal function (*SI Appendix*, Fig. S9 *A* and *C*).

Biological Pathways during the Development of Foveal Cones. A hallmark of postnatal maturation in foveal cones is the drastic morphological changes that they undergo. At birth, foveal cones are immature cuboidal cells arranged in one or two layers without obvious outer segments or axons (40, 41). As the fovea matures, they migrate centripetally, pack into ten somatic layers, develop long, slender outer segments and extend long axons (42) (Fig. 1*B*). To investigate the molecular changes associated with these developmental alterations, we pooled all 7,198 cones (foveal and peripheral from neonates and adults) and performed an unsupervised clustering of the dataset. They formed four discrete clusters, precisely divided by age and region (Fig. 7*A*).

We used the GO-PCA analysis (43) to find biological pathways that distinguished cones by age or region (Fig. 7*B* and *SI Appendix*,

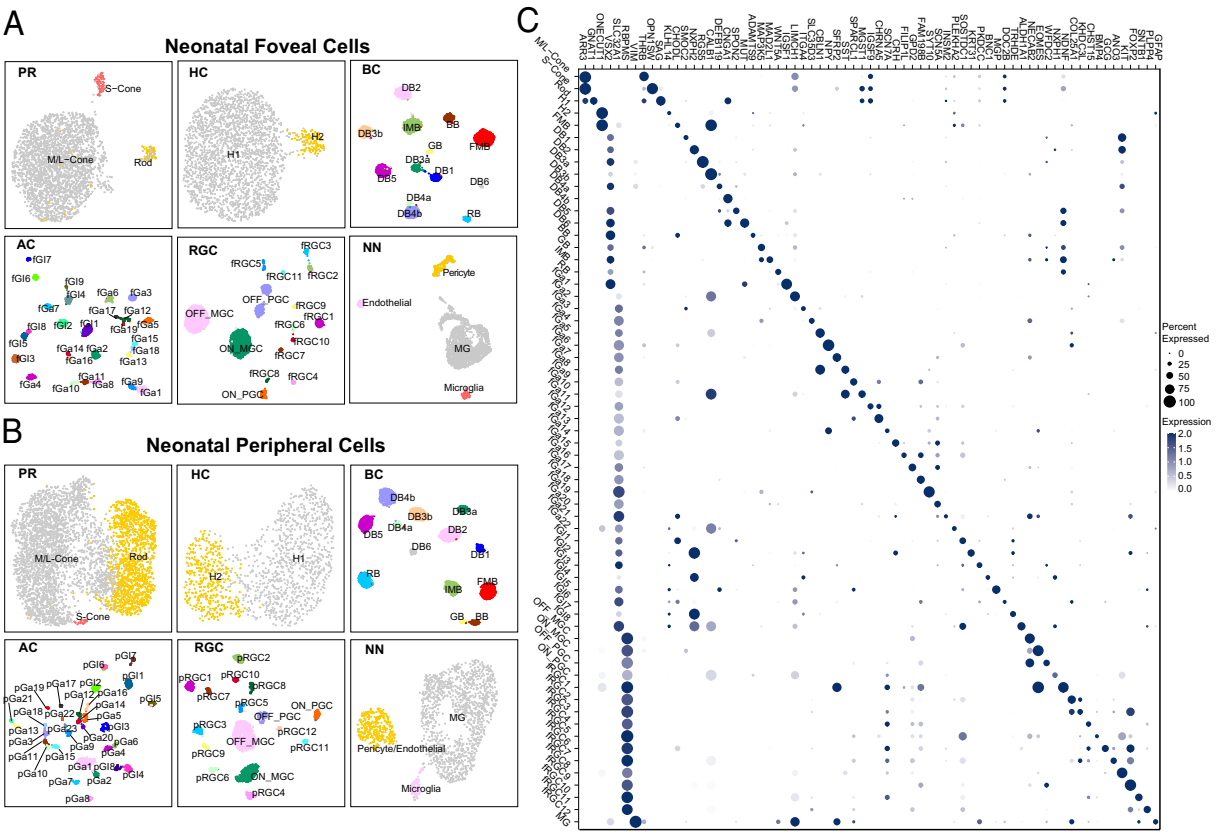

Fig. 4. Cell atlas of the neonatal marmoset retina. (*A*) UMAP visualization of cell types in the fovea of neonatal marmoset. (*B*) UMAP visualization of cell types in the peripheral retina of neonatal marmoset. (*C*) Dot plot showing the expression of marker genes for individual foveal cell classes (*Left* seven columns) and types (remaining columns).

Fig. S9*E*). Neonatal foveal cones were enriched over neonatal peripheral cones, as well as all adult cones, in pathways associated with active morphogenesis such as "axon-dendritic transport," "cytoskeleton-dependent intracellular transport," and "protein localization to plasma membrane." This result is consistent with the relatively immature state of foveal cones at birth. In adults, foveal and peripheral cones differed in pathways related to energy metabolism: Adult foveal cones were enriched over all other groups in genes involved in glycolysis and gluconeogenesis, whereas adult peripheral cones were enriched over all other groups in pathways involved in oxidative phosphorylation, such as ATP coupled electron transport and proton-transporting ATP synthase complex. This difference raises the possibility that foveal and peripheral cones are powered in different ways (44).

Interestingly, the GO term "photoreceptor cell maintenance" identified multiple genes linked to retinitis pigmentosa (45) and Leber Congenital Amaurosis (LCA) (46) as selectively enriched in foveal cones (*SI Appendix*, Fig. S9*E*). Of note, retinal dehydrogenase 12 (*RDH12*), the causal gene for LCA13, was differentially expressed between foveal and peripheral cones at the neonatal stage, but the regional difference evened out by adulthood (SI Appendix, Fig. S9 *E* and *F*). Although LCA13 affects the entire eye, macular dystrophy is an early and common feature (47). This result suggests that some genes associated with macular dystrophy may exert their effects at an early stage.

Distinct Transcriptional Regulations in Neonatal Foveal and Peripheral Cones. Due to the distinct gene expression pattern of neonatal foveal cones, we used the single-cell regulatory network inference and clustering algorithm to identify region-specific gene regulatory networks that could regulate their differentiation (48). This method generates selectively regulated gene sets called regulons that contain TFs and their predicted target genes. We identified 219 regulons associated with 4,986 neonatal cones (*SI Appendix*, *Materials and Methods* and Fig. S10*A*). Regulon activity, like DEGs generally, separated neonatal cones into foveal and peripheral cohorts (Fig. 7*C*), demonstrating that some regulatory networks are differentially expressed in the two populations. The top regulons in each group are shown in Fig. 7*D*. The five regulons most enriched in foveal cones are AHR, PBX1, SOX6, BACH1, and FOXO3 as their defining TFs, while those most enriched in peripheral cones are defined by SOX4, RAX, LHX3, FOSB, and OLIG. Indeed, in many of these regulons, the key TFs and their target genes, whether positively or negatively regulated, show distinct enrichments between foveal and peripheral cones (*SI Appendix*, Fig. S10*B*). Hierarchical clustering of cones based on these five regulons confirmed a predominant separation by regions (*SI Appendix*, Fig. S10*C*). Notably, some of these TFs show differential expressions only at the neonatal stage, not in adults, suggesting their roles during the development (*SI Appendix*, Fig. S10*D*). Using FISH, we confirmed the expression of *SOX6* in foveal cones and the expressions of *SOX4* and *RAX* in peripheral cones at the neonatal retina (Fig. 7*E* and *SI Appendix*, Fig. S10*E*).

To verify the regulons inferred from scRNA-seq dataset, we generated single-cell ATAC-seq analyses of neonatal foveal and peripheral retina and identified open chromatin peaks associated with six main neuronal classes, including cones (Fig. 7 *F* and *G* and *SI Appendix*, Fig. S10*F*). The clustering of all cones separated them into two clusters, representing foveal and peripheral cones, respectively (Fig. 7*H*). Comparing the chromatin accessibility associated with the gene body and promoter regions of the TFs from the top regulons, we found that *SOX6*, *AHR*, and *BACH1* show

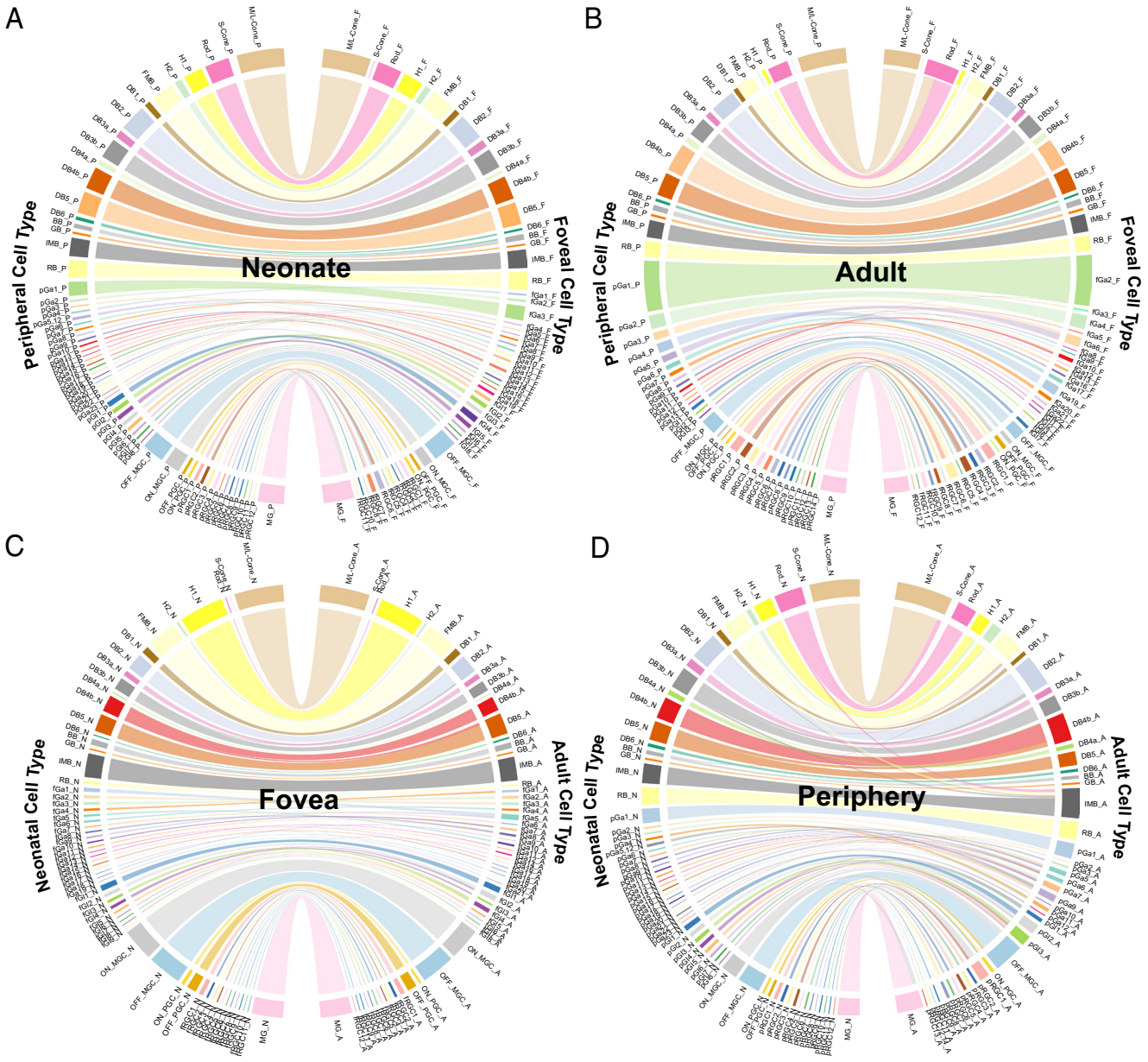

Fig. 5. Transcriptomic correspondences of cell types across retinal regions and across developmental stages. (*A*) Chord diagram showing transcriptomic correspondence between foveal and peripheral cells in the neonatal stage. (*B*) Chord diagram showing transcriptomic correspondence between foveal and peripheral cells in the adult stage. (*C*) Chord diagram showing transcriptomic correspondence between neonatal and adult retinal cells in the fovea. (*D*) Chord diagram showing transcriptomic correspondence between neonatal and adult retinal cells in the peripheral retina. Each line maps a cell type on the left to its corresponding type on the right, and the width of each bar reflects the cell number. Cell types are ordered from top to bottom as PRs, HCs, BCs, ACs, RGCs, and MG. The detailed correspondence is listed in *SI Appendix*, Table S4. The names of cell types are consistent with those identified in Figs. 2 and 4.

higher gene activities in foveal cones, while *LHX3*, *FOSB*, *RAX*, and *SOX4* have higher activities in peripheral cones, consistent with their regulon activities (Fig. 7*I*). We further determined the enriched motif binding sites of TFs associated with differential peaks between foveal and peripheral cones. Among the TFs with significant binding motifs, six TFs are matched with top regulons (Fig. 7*J*). Altogether, these results verify most of the inferred regulons and demonstrate distinct transcriptional regulation in foveal and peripheral cones.

Predicted Interactions between Foveal MG and Cones. We next turned to MG because, as noted above, they and cones show the greatest regional and developmental differences among cell types (Fig. 6 and *SI Appendix*, Fig. S8 *C* and *D*). This pattern suggests the possibility that MG maturation could promote cone maturation. Thus, we first investigated the potential biological functions associated with genes differentially expressed between neonatal foveal and peripheral MG (referred to as regional DEGs). By performing protein–protein interaction (PPI) analysis of these regional DEGs, we can identify closely connected components via the Molecular Complex Detection (MCODE) algorithm, which aids in identifying functional modules within regional DEGs (*SI Appendix*, *Materials and Methods*). Application of this method identified 13 components, annotation of which revealed 11 functional modules. Many modules are related to common cellular processes, such as oxidative phosphorylation, proteolysis, and mRNA processing. However, three modules—1) Regulation of growth (*STAT1*, *INSR*, *FGF9*, and *FGF13*), 2) Regulation of insulin-like growth factor (*IGFBP4*, *IGFBP5*, and *SPP1*), and 3) collagen biosynthesis and extracellular matrix organization

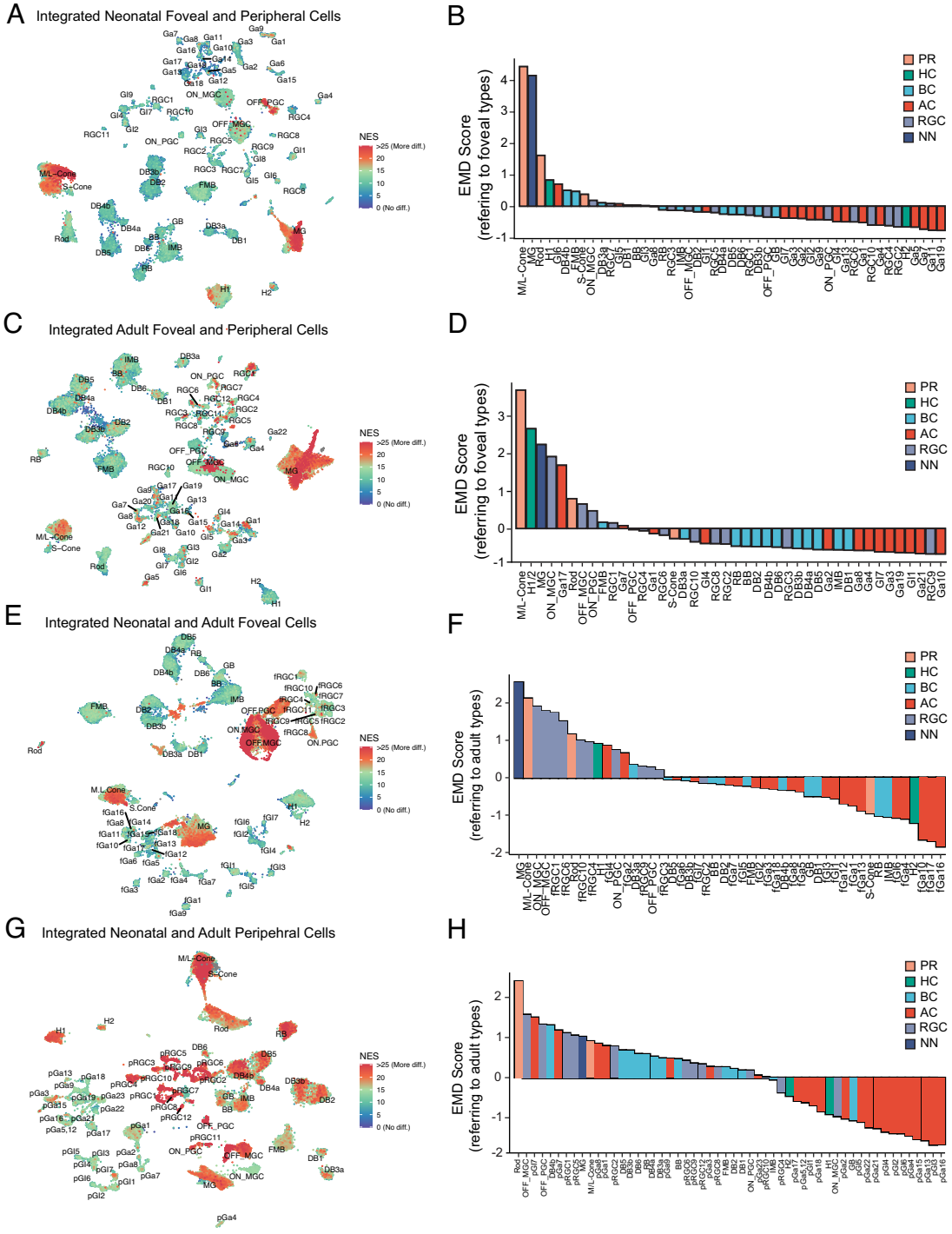

Fig. 6. Transcriptomic comparisons of cell types across retinal regions and across developmental stages. (*A*) UMAP visualization of regional differences measured by NES in individual foveal and peripheral cells, integrated at the neonatal stage. (*B*) Bar plot showing regional differences measured by scaled EMD scores in integrated foveal and peripheral cell types at the neonatal stage. (*C*) UMAP visualization of regional differences measured by NES scores in individual foveal and peripheral cells, integrated at the adult stage. (*D*) Bar plot showing regional differences measured by EMD scores in integrated foveal and peripheral cell types at the adult stage. (*E*) UMAP visualization of developmental changes measured by NES scores in individual neonatal and adult cells, integrated at the foveal region. (*F*) Bar plot showing developmental changes measured by EMD scores in integrated neonatal and adult cell types at the foveal region. (*G*) UMAP visualization of developmental changes measured by NES scores in individual neonatal and adult cells, integrated at the peripheral region. (*H*) Bar plot showing developmental changes measured by EMD scores in integrated neonatal and adult cell types at the peripheral region. The NES values are divided into three ranges: low (0 to 10), medium (10 to 20), and high (above 20). The correspondence between the names of integrated cell types and those at each stage are listed in *SI Appendix*, Table S5 for *A* and *C*, and in *SI Appendix*, Table S6 for *E* and *G*.

(*COL2A1*, *COL4A3*, *COL4A4*, *COL9A1*, and *COL11A1*)—are of interest as they suggest a potential role of MG in morphogenesis (Fig. 8 *A* and *C*). We validated expression of some of these regional DEGs by in situ hybridization (Fig. 8*B*).

In seeking MG-derived factors that could affect cones, we noted that several of the genes most enriched in neonatal foveal MG were secreted molecules known to interact with cellular receptors, including FGF9, FGF13, CTGF, VEGFA, SPP1, and several collagens. We therefore employed the computational method NicheNet (49) to predict the secreted ligands from MG that could influence the expression of genes enriched in foveal cones. First, we imputed all potential ligand–receptor pairs

between foveal MG and foveal cones using the NicheNet prior model (*SI Appendix*, Fig. S11*A*). We then prioritized top active ligands based on their ligand activities, which are calculated by a statistical correlation between predicated expressions of target genes as downstream effects from each ligand–receptor interaction and the real expression levels of target genes. Among the 19 top-ranked ligands, we found five that broadly drive the expression of enriched genes in foveal cones, with many of these target genes being involved in cytoskeleton movement and cilium assembly (Fig. 8*D*). In contrast, when we used NicheNet to explore the opposite regulatory direction, namely secreted ligands from foveal cones that might influence expression of genes enriched in foveal MG, we found weaker ligand activity of foveal cones compared to MG, and few cases in which cone-derived ligands were predicted to drive expression of MG genes (*SI Appendix*, Fig. S11 *B* and *C*). This asymmetry suggests the possibility that proteins secreted from neonatal foveal MG may play a role in the maturation of foveal cones, thereby providing a foundation for future mechanistic studies of foveal maturation (Fig. 8*C*).

Discussion

It is important to study the retina of nonhuman primates because they share features with humans that are absent from other model systems, such as mice. The fovea is one prominent primate-specific structure. In this context, marmosets are of growing interest because their small bodies and relatively short gestation period suit them for biomedical research generally and vision science in particular (16). Despite previous histological and physiological characterization of marmoset retinal cell types (18, 21), the overall cellular composition of the marmoset retina remains undefined. We utilized scRNA-seq to characterize the cell types in the fovea and peripheral retina of both adult and neonatal marmosets and compared them to those of macaque and human. The cell types we identified are transcriptomically related across regions, ages, and species, but each comparison revealed intriguing differences in gene expression. This study provides a cell atlas of the marmoset retina that will facilitate primate retinal research and enable further analysis of foveal evolution and maturation.

Foveal Evolution. Marmosets are considered a more primitive primate species than macaque and humans, as marmosets have a smaller and smoother-surfaced brain (50). We suspected that marmosets might have a simpler fovea than humans or macaques, with cell types similar to those in a hypothetical primate ancestor. However, our cross-primate comparisons suggest a different model. First, the marmoset contains a large diversity of cell types, no fewer than those reported in macaques or humans (Figs. 2 and 3). Moreover, the transcriptomic profile of foveal cell types displayed a high degree of correspondence across marmosets, macaques, and humans (Fig. 3). Last, fractions of individual foveal cell types are comparable between these three species (*SI Appendix*, Table S3). These results indicate that a pool of diverse cell types may have been established when the foveated primate ancestor emerged 35 to 40 Mya. Notably, foveal size is almost uniform across primates, despite a large variation in total retinal area from marmosets to humans (9). These conserved features suggest that the primate fovea shares a common blueprint, and that its conserved cellular and molecular composition is critical for constructing a functional foveal circuit to support high-acuity vision. Furthermore, the conserved nature of the marmoset fovea suggests that it may be particularly valuable for the study of macular degeneration and dystrophy (7, 22).

Despite the high degree of conservation of the primate fovea, several species-specific differences exist. A subtle but critical difference is that the marmoset fovea contains the lowest fraction of midget RGCs (MGCs) among the three primate species (Fig. 3). This finding is consistent with the fact that the marmoset has fewer laminated parvocellular layers that receive projections from MGCs compared to the macaque, but has a well-defined lamination of the koniocellular layer where other RGCs innervate (51, 52). In the midget pathway, the fraction of ON MGCs and the BCs that innervate them (called invaginating midget BCs or IMBs) showed increased dominance from marmoset to macaque to human. However, this pattern was not observed for the OFF MGCs or the bipolars that innervate them (flat midget BCs or FMBs). Thus, the modification of ON and OFF midget pathways may have occurred via distinct evolutionary trajectories. Supporting this hypothesis, a recent study using serial block-face scanning electron microscopy identified S-cone specific FMB in the human retina and macaque, but not in marmoset (53). Thus, the OFF midget pathway gained additional circuit connections for color vision in macaque and human but not in marmoset (54). The transcriptomic identification of OFFx BCs in the macaque and human fovea but not in the marmoset is also intriguing. Transcriptomic mapping has confirmed that OFFx BC is a homolog of a mouse BC type (BC1B) (26, 35, 37), suggesting that it may have been lost in marmoset.

Foveal Development. By using regional scores to calculate the transcriptomic divergence in corresponding cell types between the fovea and peripheral retina, we identified several key themes of the foveal development. First, nearly all retinal cell types are fully specified at birth in both the fovea and peripheral retina (Fig. 5 *C* and *D*). Second, the level of regional transcriptomic difference is not uniform across cell types, but rather more prominent in a few of select cell types (Fig. 6 *A*–*D*). Third, regional differences increased during postnatal development (*SI Appendix*, Fig. S8*C*). Fourth, the level of developmental change is not uniform across cell types, with only selected cell types undergoing drastic developmental changes (Fig. 6 *E*–*H* and *SI Appendix*, Fig. S8*D*).

Interestingly, the top three cell types showing the greatest regional and developmental differences are foveal MG, cones, and MGCs (Fig. 6 *A*–*F*). These three cell types undergo active modifications that facilitate foveal maturation. For example, in foveal cones, enriched biological pathways include cytoskeleton modification and photoreceptor development (Fig. 7*B*), which align with forthcoming morphological changes of foveal cones and are hallmark events that lead to foveal maturation (Fig. 1*B*).

Gene expression differences between foveal and peripheral cells are likely influenced by their local environment and controlled by distinct transcriptional regulation programs. Notably, foveal and peripheral cones showed divergent transcriptional regulation at the neonatal age. Among the top enriched TFs, a pair of Sry-related box transcription factors—SOX6 and SOX4—and their regulated downstream genes, are expressed in foveal and peripheral cones, respectively (Fig. 7*D* and *SI Appendix*, Fig. S10 *B* and *C*). The distinct expressions and gene activities of SOX6 and SOX4 between foveal and peripheral cones are confirmed by FISH and scATAC-seq, respectively (Fig. 7 *E* and *I* and *SI Appendix*, Fig. S10*E*). Notably, active motif activities of SOX4 were detected in peripheral cones (Fig. 7*J*). SOX4 has been shown to mediate retinal development, while the role of SOX6 in the retina is unknown (55, 56). Interestingly, the expression of SOX6 and SOX4 is transient in cones as their expression is not detected in adults (*SI Appendix*, Fig. S10*D*), pointing to the importance of the early postnatal period for the transcriptional programs that lead to foveal maturation. Defects in acquiring the specific transcriptional machinery could cause altered

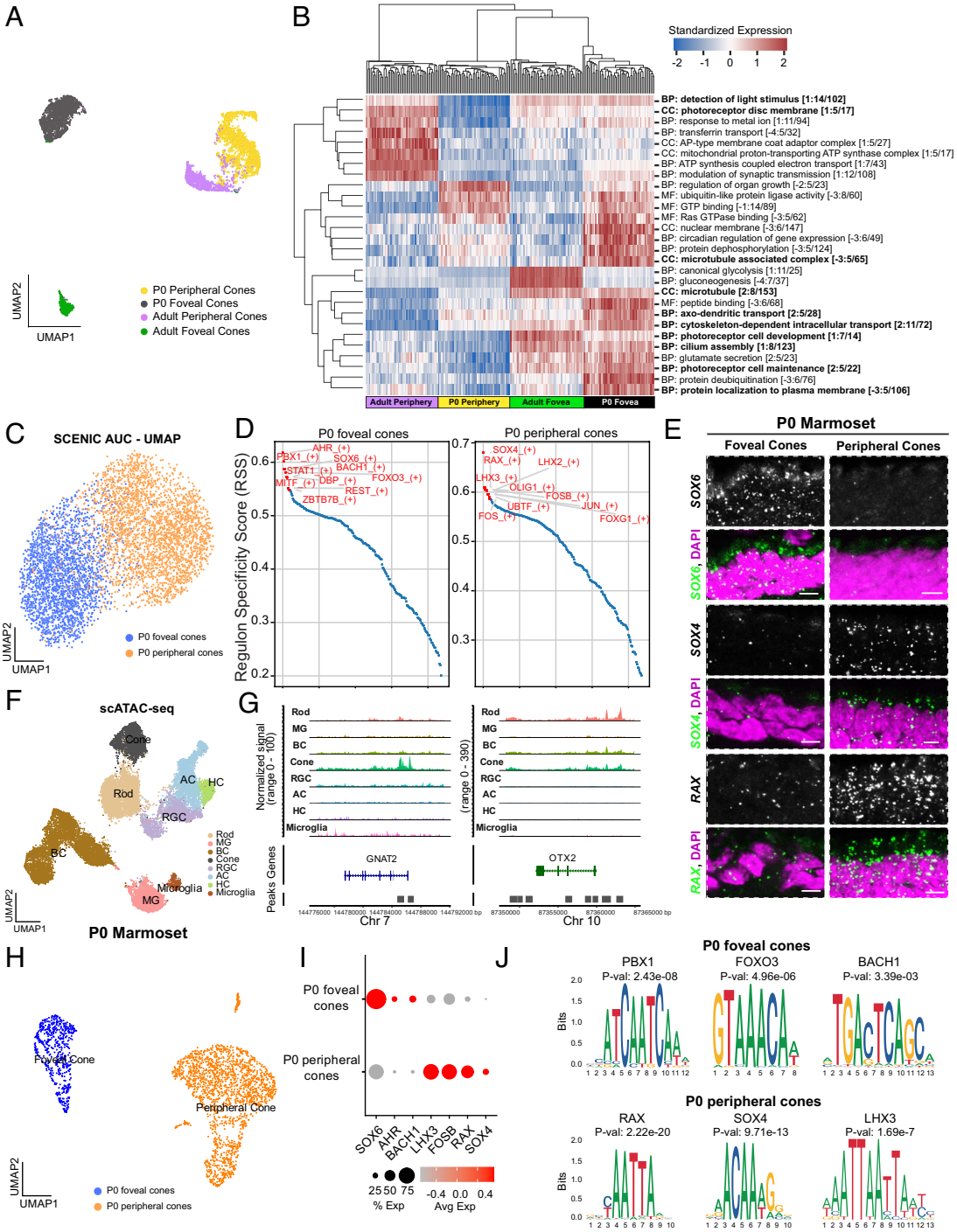

Fig. 7. Distinct biological pathways and transcriptional landscapes associated with distinct cone types. (*A*) UMAP visualization of four cone clusters, each representing either foveal or peripheral cones at either neonatal (P0) or adult stage. (*B*) Heatmap of significant Gene Ontology (GO) terms (BP, biological processes; CC, cellular component; MF, molecular function) from GO-PCA analysis. Ten GO terms related to cytoskeleton changes or photoreceptor function and development are highlighted in bold. (*C*) UMAP visualization of regulon (i.e., a gene regulatory group consisting of a transcriptional factor and its downstream regulated genes) activities showing a separation of neonatal foveal and peripheral cones. (*D*) Waterfall plot showing the top ten regulons ranked by Regulon Specificity Score in neonatal foveal and peripheral cones, respectively. (*E*) Fluorescence in situ hybridization (FISH) validation of the expression of *SOX6, SOX4, and RAX* (green) in neonatal cones. Nuclei stained with DAPI are in magenta. (Scale bar, 5 μm.) (*F*) UMAP visualization of cell classes identified from scATAC-seq data at P0. (*G*) Coverage plots showing peaks enriched at the loci of known cone marker genes, *GNAT2* and *OTX2*, across all cell classes. (*H*) UMAP visualization of P0 foveal and peripheral cones from scATAC-seq data. (*I*) Dot plot showing the chromatin accessibility of selected transcription factors (TFs) between foveal and peripheral cones. (*J*) Identification of significantly enriched TF binding motifs associated with differential accessible peaks between foveal and peripheral cones.

foveal development, as observed in pediatric patients with retinopathy of prematurity (57). Furthermore, some of the identified TFs' functions align with characteristic features of the fovea. For example, the BACH1 regulatory network is enriched in neonatal foveal cones (Fig. 7 *D* and *I* and *SI Appendix*, Fig. S10 *B* and *C*). BACH1 is known to repress Wnt/β-Catenin signaling and angiogenesis, which may be critical for maintaining the avascular area around the fovea (58). Future studies on the roles of these TFs in neonatal foveal cone maturation may open avenues for the application of foveal cone differentiation in translational settings.

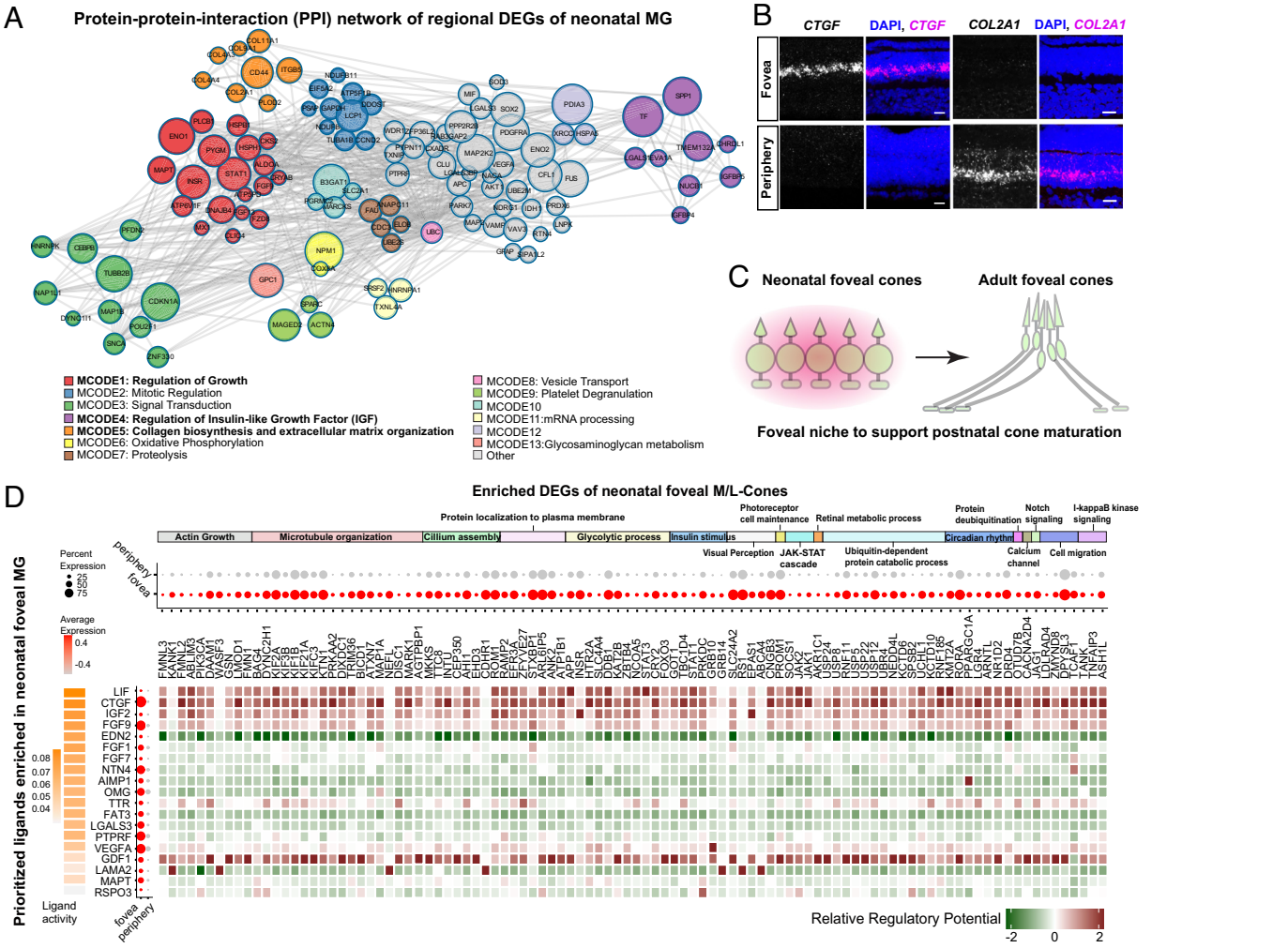

Fig. 8. Potential interactions between foveal MG and cones. (*A*) PPI network analysis of DEGs between neonatal foveal and peripheral MG showing densely connected network components, which are involved in multiple growth-related GO terms. Each line indicates interactions between two proteins, while the circle size represents the connectivity degree, with larger circles indicating a higher degree. Distinct MCODE components are color-coded, and annotations of MCODE components to functional modules are listed. "Other" means no MCODE complex detected. No functional modules are associated with MCODE 10 and 12. MCODE1, 4, and 5 are highlighted in bold. (*B*) FISH validations of *CTGF* (magenta) and *COL2A1* (magenta) expression in foveal and peripheral MG, respectively. Nuclei stained with DAPI are in blue. (Scale bar, 20 μm.) (*C*) A working model suggesting that the fovea provides a specific niche which enables the morphogenesis of postnatal cones. (*D*) NicheNet analysis predicting potential communication pathways between MG and cones. From left to right: orange heatmap showing the ranked ligand activity of nineteen ligands (secreted or membrane-bound) that are enriched in foveal MG; dot plot showing the expression of these ligands in the neonatal MGs; heatmap of the ligand–target interaction matrix denoting the relative regulatory potential between ligands from foveal MG and their target genes in foveal cones. From *Top* to *Bottom*: annotation bars grouping the target genes in foveal cones based on GO terms; dot plot showing the expression of these target genes in neonatal foveal cones.

The Role of MG in Foveal Development. Regional heterogeneity of MG has been observed in the chicken retina. Specifically, chicken MG shows transcriptomic heterogeneity associated with their cardinal positions in the retina (59). Particularly in the high acuity area (HAA), a rod-free zone in the chicken retina, MG expresses a high level of FGF8, CYP26C1, and CYP26A1 (60). The enriched expression of these three genes is important for maintaining a low level of retinoic acid, which inhibits the fate of rods but promotes cone fate in the HAA. Thus, MG at distinct retinal locations could maintain a specific environmental niche to guide regional neurogenesis and neuronal development.

Previous studies of the macaque and human retina have identified a significant degree of difference in gene expression between foveal and peripheral MG (26, 27, 61). In this study of the marmoset retina, MG are also the most divergent cell type between the fovea and peripheral retina (Fig. 6 *A*–*D* and *SI Appendix*, Fig. S8*C*). Thus, MG maintain a distinct molecular profile in the primate fovea. Many of these genes enriched in foveal MG, such as FGF9, are shared across primates, suggesting a conserved role in supporting foveal function (*SI Appendix*, Fig. S9*D*). Furthermore, cell–cell interaction analysis via NicheNet predicted a strong regulation of gene expression in foveal cones by secreted ligands, such as FGF9 and CTGF (Fig. 8*D*). FGF9 is particularly interesting in that FGF signaling mediates the development of the outer plexiform layer in the zebrafish retina (62), and FGF receptors have enriched expression in primate foveal cones (63). Future confirmation of the source of FGF9 and an in vivo examination of the function of FGF9 are necessary to determine the role of foveal MG in mediating the cone morphogenesis.

Materials and Methods

Tissue Procurement and Sequencing Library Preparation. Adult and neonatal eyes were enucleated from deeply anesthetized male and female marmosets (around 2 y old) at the time of death. All the neonatal eyes used in the study were obtained from postnatal day zero (P0) marmosets. The marmoset tissue collection was approved by and in accordance with the guidelines for the care and use of animals at Massachusetts Institute of Technology Institutional Animal Care and Use Committee. Marmoset eyes were collected from animals that had reached the end of unrelated studies. No ocular or visual abnormalities were noted. After enucleation, eyes were

immediately placed in ice-cold hibernate medium (BrainBits) before dissection. The anterior chamber and the vitreous were removed by a rapid hemisection, and the posterior eyecup was immersed in room-temperature Ames' medium (Sigma, equilibrated with 95% O2/5% CO2 for at least 20 min). For details of dissection, library preparation for scRNA-seq, snRNA-seq, and scATAC-seq, data analysis, FISH validations and Image Processing, see *SI Appendix, Materials and Methods*.

Data, Materials, and Software Availability. RNA sequencing data have been deposited in GEO (GSE249004)(64). Code availability: https://github.com/PengYRLab/MarmosetRetinalCellAtlas (65).

ACKNOWLEDGMENTS. This work was supported by departmental startup funds from the UCLA, a career development award from Research to Prevent Blindness, a career starter award from Knights Templar Foundation, and Klingenstein-Simons neuroscience fellowship (Y.-R.P.), and an unrestricted grant to the Department of Ophthalmology from Research to Prevent Blindness, and NIH grants EY028633 and EY022073 (J.R.S.). The marmoset resource was supported by the Yang-Tan Collective at MIT, Tan-Yang Center for Autism Research at MIT, the Stanley Center for Psychiatric Research at Broad Institute of MIT and Harvard. We thank Raneesh Ramarapu for assisting with initial data analysis and technical assistance.

1. E. C. Kirk, R. F. Kay, "The evolution of high visual acuity in the anthropoidea" in *Anthropoid Origins: New Visions*, C. F. Ross, R. F. Kay, Eds. (Springer, US, Boston, MA, 2004), pp. 539–602, 10.1007/978-1-4419-8873-7_20.
2. J. M. Provis, C. M. Diaz, B. Dreher, Ontogeny of the primate fovea: A central issue in retinal development. *Prog. Neurobiol.* **54**, 549–581 (1998).
3. J. M. Provis, A. M. Dubis, T. Maddess, J. Carroll, Adaptation of the central retina for high acuity vision: Cones, the fovea and the avascular zone. *Prog. Retin. Eye Res.* **35**, 63–81 (2013).
4. T. Baden, T. Euler, P. Berens, Understanding the retinal basis of vision across species. *Nat. Rev. Neurosci.* **21**, 5–20 (2020).
5. A. Hendrickson, "Organization of the adult primate fovea" in *Macular Degeneration*, P. L. Penfold, J. M. Provis, Eds. (Springer Berlin Heidelberg, Berlin, 2005), pp. 1–23, 10.1007/3-540-26977-0_1.
6. A. Bringmann *et al.*, The primate fovea: Structure, function and development. *Prog. Retin. Eye Res.* **66**, 49–84 (2018).
7. A. C. Bird, D. Bok, Why the macula? *Eye (Lond.)* **32**, 858–862 (2018).
8. R. Nuzzi, L. Dallorto, A. Vitale, Cerebral modifications and visual pathway reorganization in maculopathy: A systematic review. *Front. Neurosci.* **14**, 755 (2020).
9. U. Grünert, P. R. Martin, Cell types and cell circuits in human and non-human primate retina. *Prog. Retin. Eye Res.* **78**, 100844 (2020).
10. R. H. Masland, The neuronal organization of the retina. *Neuron* **76**, 266–280 (2012).
11. S. J. Schein, Anatomy of macaque fovea and spatial densities of neurons in foveal representation. *J. Comp. Neurol.* **269**, 479–505 (1988).
12. H. D. Wilder, U. Grünert, B. B. Lee, P. R. Martin, Topography of ganglion cells and photoreceptors in the retina of a New World monkey: The marmoset Callithrix jacchus. *Vis. Neurosci.* **13**, 335–352 (1996).
13. T. L. Chan, P. R. Martin, N. Clunas, U. Grünert, Bipolar cell diversity in the primate retina: Morphologic and immunocytochemical analysis of a new world monkey, the marmoset Callithrix jacchus. *J. Comp. Neurol.* **437**, 219–239 (2001).
14. R. Sinha *et al.*, Cellular and circuit mechanisms shaping the perceptual properties of the primate fovea. *Cell* **168**, 413–426.e2 (2017).
15. G. S. Bryman, A. Liu, M. T. H. Do, Optimized signal flow through photoreceptors supports the high-acuity vision of primates. *Neuron* **108**, 335–348.e7 (2020).
16. J. F. Mitchell, D. A. Leopold, The marmoset monkey as a model for visual neuroscience. *Neurosci. Res.* **93**, 20–46 (2015).
17. H. Okano, Current status of and perspectives on the application of marmosets in neurobiology. *Annu. Rev. Neurosci.* **44**, 27–48 (2021).
18. P. R. Jusuf, S. C. S. Lee, J. Hannibal, U. Grünert, Characterization and synaptic connectivity of melanopsin-containing ganglion cells in the primate retina. *Eur. J. Neurosci.* **26**, 2906–2921 (2007).
19. C. J. Abbott, K. A. Percival, P. R. Martin, U. Grünert, Amacrine and bipolar inputs to midget and parasol ganglion cells in marmoset retina. *Vis. Neurosci.* **29**, 157–168 (2012).
20. A. J. Chandra, S. C. S. Lee, U. Grünert, Melanopsin and calbindin immunoreactivity in the inner retina of humans and marmosets. *Vis. Neurosci.* **36**, E009 (2019).
21. R. A. Masri, K. A. Percival, A. Koizumi, P. R. Martin, U. Grünert, Survey of retinal ganglion cell morphology in marmoset. *J. Comp. Neurol.* **527**, 236–258 (2019).
22. S. Picaud *et al.*, The primate model for understanding and restoring vision. *Proc. Natl. Acad. Sci. U.S.A.* **116**, 26280–26287 (2019).
23. U. Grünert *et al.*, Retinal ganglion cells projecting to superior colliculus and pulvinar in marmoset. *Brain Struct. Funct.* **226**, 2745–2762 (2021).
24. R. F. Kay, New World monkey origins. *Science* **347**, 1068–1069 (2015).
25. Y. Shao *et al.*, Phylogenomic analyses provide insights into primate evolution. *Science* **380**, 913–924 (2023).
26. Y. R. Peng *et al.*, Molecular classification and comparative taxonomics of foveal and peripheral cells in primate retina. *Cell* **176**, 1222–1237.e22 (2019).
27. W. Yan *et al.*, Cell atlas of the human fovea and peripheral retina. *Sci. Rep.* **10**, 1–17 (2020).
28. G. X. Y. Zheng *et al.*, Massively parallel digital transcriptional profiling of single cells. *Nat. Commun.* **8**, 14049 (2017).
29. N. M. Tran *et al.*, Single-cell profiles of retinal ganglion cells differing in resilience to injury reveal neuroprotective genes. *Neuron* **104**, 1039–1055.e12 (2019).
30. W. Yan *et al.*, Mouse retinal cell atlas: Molecular identification of over sixty amacrine cell types. *J. Neurosci.* **40**, 5177–5195 (2020).
31. A. Butler, P. Hoffman, P. Smibert, E. Papalexi, R. Satija, Integrating single-cell transcriptomic data across different conditions, technologies, and species. *Nat. Biotechnol.* **36**, 411–420 (2018).
32. J. S. Diamond, Inhibitory interneurons in the retina: Types, circuitry, and function. *Annu. Rev. Vis. Sci.* **3**, 1–24 (2017).
33. M. T. H. Do, Melanopsin and the intrinsically photosensitive retinal ganglion cells: Biophysics to behavior. *Neuron* **104**, 205–226 (2019).
34. M. L. Aranda, T. M. Schmidt, Diversity of intrinsically photosensitive retinal ganglion cells: Circuits and functions. *Cell. Mol. Life Sci.* **78**, 889–907 (2021).
35. L. Della Santina *et al.*, Glutamatergic monopolar interneurons provide a novel pathway of excitation in the mouse retina. *Curr. Biol.* **26**, 2070–2077 (2016).
36. K. Shekhar *et al.*, Comprehensive classification of retinal bipolar neurons by single-cell transcriptomics. *Cell* **166**, 1308–1323.e30 (2016).
37. J. Hahn *et al.*, Evolution of neuronal cell classes and types in the vertebrate retina. *Nature* **624**, 415–424 (2023).
38. T. Chen, C. Guestrin, "Xgboost: A scalable tree boosting system" in *Proceedings of the 22nd ACM SIGKDD International Conference on Knowledge Discovery and Data Mining* (Association for Computing Machinery, San Francisco, California, USA, 2016), pp. 785–794.
39. D. Y. Orlova *et al.*, Earth mover's distance (EMD): A true metric for comparing biomarker expression levels in cell populations. *PLoS One* **11**, e0151859 (2016).
40. A. Hendrickson, D. Troilo, D. Possin, A. Springer, Development of the neural retina and its vasculature in the marmoset Callithrix jacchus. *J. Comp. Neurol.* **497**, 270–286 (2006).
41. A. Hendrickson, C. Zhang, Development of cone photoreceptors and their synapses in the human and monkey fovea. *J. Comp. Neurol.* **527**, 38–51 (2019).
42. A. D. Springer, D. Troilo, D. Possin, A. E. Hendrickson, Foveal cone density shows a rapid postnatal maturation in the marmoset monkey. *Vis. Neurosci.* **28**, 473–484 (2011).
43. F. Wagner, GO-PCA: An unsupervised method to explore gene expression data using prior knowledge. *PLoS One* **10**, e0143196 (2015).
44. N. T. Ingram, G. L. Fain, A. P. Sampath, Elevated energy requirement of cone photoreceptors. *Proc. Natl. Acad. Sci. U.S.A.* **117**, 19599–19603 (2020).
45. D. T. Hartong, E. L. Berson, T. P. Dryja, Retinitis pigmentosa. *Lancet* **368**, 1795–1809 (2006).
46. S. H. Tsang, T. Sharma, Leber congenital amaurosis. *Adv. Exp. Med. Biol.* **1085**, 131–137 (2018).
47. H. Sarkar, M. Moosajee, Retinol dehydrogenase 12 (RDH12): Role in vision, retinal disease and future perspectives. *Exp. Eye Res.* **188**, 107793 (2019).
48. B. Van de Sande *et al.*, A scalable SCENIC workflow for single-cell gene regulatory network analysis. *Nat. Protoc.* **15**, 2247–2276 (2020).
49. R. Browaeys, W. Saelens, Y. Saeys, NicheNet: Modeling intercellular communication by linking ligands to target genes. *Nat. Methods.* **17**, 159–162 (2020).
50. S. G. Solomon, M. G. P. Rosa, A simpler primate brain: The visual system of the marmoset monkey. *Front. Neural Circuits.* **8**, 96 (2014).
51. K. A. Percival, P. R. Martin, U. Grünert, Organisation of koniocellular-projecting ganglion cells and diffuse bipolar cells in the primate fovea. *Eur. J. Neurosci.* **37**, 1072–1089 (2013).
52. N. Zeater, S. K. Cheong, S. G. Solomon, B. Dreher, P. R. Martin, Binocular visual responses in the primate lateral geniculate nucleus. *Curr. Biol.* **25**, 3190–3195 (2015).
53. Y. J. Kim *et al.*, Comparative connectomics reveals noncanonical wiring for color vision in human foveal retina. *Proc. Natl. Acad. Sci. U.S.A.* **120**, e2300545120 (2023).
54. S. C. S. Lee, I. Telkes, U. Grünert, S-cones do not contribute to the OFF-midget pathway in the retina of the marmoset, Callithrix jacchus. *Eur. J. Neurosci.* **22**, 437–447 (2005).
55. T. Kuwajima, C. A. Soares, A. A. Sitko, V. Lefebvre, C. Mason, SoxC transcription factors promote contralateral retinal ganglion cell differentiation and axon guidance in the mouse visual system. *Neuron* **93**, 1110–1125.e5 (2017).
56. F. Wu *et al.*, Single cell transcriptomics reveals lineage trajectory of retinal ganglion cells in wild-type and Atoh7-null retinas. *Nat. Commun.* **12**, 1465 (2021).
57. J. D. Akula *et al.*, The fovea in retinopathy of prematurity. *Investig. Ophthalmol. Vis. Sci.* **61**, 28–28 (2020).
58. L. Jiang *et al.*, Bach1 represses Wnt/β-catenin signaling and angiogenesis. *Circ. Res.* **117**, 364–375 (2015).
59. M. Yamagata, W. Yan, J. R. Sanes, A cell atlas of the chick retina based on single-cell transcriptomics. *ELife* **10**, e63907 (2021).
60. S. da Silva, C. L. Cepko, Fgf8 expression and degradation of retinoic acid are required for patterning a high-acuity area in the retina. *Dev. Cell.* **42**, 68–81.e6 (2017).
61. T. Zhang *et al.*, Human macular Müller cells rely more on serine biosynthesis to combat oxidative stress than those from the periphery. *Elife.* **8**, e43598 (2019).
62. S. Hochmann *et al.*, Fgf signaling is required for photoreceptor maintenance in the adult zebrafish retina. *PLoS One* **7**, e30365 (2012).
63. E. E. Cornish, R. C. Natoli, A. Hendrickson, J. M. Provis, Differential distribution of fibroblast growth factor receptors (FGFRs) on foveal cones: FGFR-4 is an early marker of cone photoreceptors. *Mol. Vis.* **10**, 1–14 (2004).
64. L. Zhang *et al.*, Evolutionary and developmental specialization of foveal cell types in the marmoset. NCBI GEO. https://www.ncbi.nlm.nih.gov/geo/query/acc.cgi?acc=GSE249004. Deposited 30 November 2023.
65. L. Zhang *et al.*, Data from "Evolutionary and Developmental specialization of foveal cell types in the marmoset." Github Repository. https://github.com/PengYRLab/MarmosetRetinalCellAtlas. Deposited 27 February 2024.